CHEMICAL ENGINEERING TRANSACTIONS
VOL. 88, 2021
A publication of AIDIC
The Italian Association of Chemical Engineering
Online at www.cetjournal.it
Guest Editors: Petar S. Varbanov, Yee Van Fan, Jiří J. Klemeš

ISBN 978-88-95608-86-0; **ISSN** 2283-9216
DOI: 10.3303/CET2188152

Modelling of Physical Method for Tar Elimination from Producer Gas at Low Temperature

Rita Harb[a,b], Rodrigo Rivera-Tinoco[a], Barbar Zeghondy[b], Chakib Bouallou[a,*]

[a] MINES ParisTech, PSL Research University, Center for Energy Efficiency of Systems (CES), 60 Bd St Michel, F-75006 Paris, France
[b] School of Engineering, Holy Spirit University of Kaslik (USEK), Jounieh, Lebanon
chakib.bouallou@mines-paristech.fr

Combining a methanation step with biomass gasification requires an intensive tar removal process that reduces its content down to 1 mg/Nm^3. In this paper, low temperature processes are suggested for treating tar and reducing its content to the acceptable limit. However, the gas must be pre-treated prior to the low temperature process in order to reduce its temperature, its moisture content and the heavy tar fraction. Two water scrubbers are placed prior to the low temperature tar removal process. Benzene and toluene remains in the producer gas after the scrubbers. Those two components can be valorised if separated from the producer gas at low temperature. The tar removal, at low temperature, induces the water vapour frosting remaining in the producer gas. The simultaneous frosting and condensation takes place over a cold plate. Modelling simultaneously the multi-component frost growth and condensation requires complex mathematical approach. A parametric study is completed to assess the impact of the wall temperature and the producer gas flow rate on the tar removal process function of time and plate length. Results showed that a wall temperature of -20 °C is required to lead to the benzene frost formation for an initial molar fraction of 0.024. After one hour, the thicknesses of benzene and ice frost layers reach 1.5 and 2.5 mm, respectively. Therefore, the heat transfer between the gas and the cold surface is reduced.

1. Introduction

Lately, production of methane based on biomass gasification is widely studied as a possible route for replacing fossil natural gas. Biomass gasification yields a gaseous product named producer gas that can be converted into bio-methane if treated (Anis and Zainal, 2011). Tars among other impurities present in the producer gas must be removed in order to successfully convert it into bio-methane. Very few researchers reached the suitable tar content for methanation (1 mg/Nm^3). Reaching a low tar content is usually achieved by combining two cleaning methods. For instance, in GoBiGas project, the polycyclic aromatic hydrocarbons (PAH) and benzene, toluene, and xylene (BTX) contents were respectively reduced to 0.1 µg/m^3 and 100 µg/m^3, by combining a scrubbing column with 4 activated carbon (AC) beds (Thunman et al., 2018). However, high operating costs are imposed by the treatment section; one of the AC beds should be replaced each 2.5 months and the oil-based scrubbing liquid is wasted. Therefore, in this study, reducing the temperature of the producer gas is suggested as an effective solution for reducing the tar content and it takes place in two units in series. The first unit targets the removal of the heavy tar fraction by scrubbers while the second unit aims at removing the lightest tar components by deposition over low temperature surfaces. The removal of the heavy fraction of tars is well developed, while more attention should be given to the removal of the lightest tar fraction formed mainly of BTX. Many previous studies have handled the tar removal by wet scrubbers using different types of scrubbing mediums (Harb et al., 2020 a). Since BTX compounds can be valorised, it is important to keep their content unaffected in this stage of tar removal while reducing the producer gas temperature and the heavy tar fraction. Therefore, water was selected as the suitable scrubbing medium although it has a removal efficiency lower than those of oily materials (Phuphuakrat et al., 2011). In order to enhance the removal efficiency, the producer gas flows through two water scrubbers placed in series. The scrubbers reduce the gas temperature from 350 to 5 °C, the molar water fraction from 0.295 to 0.009 and the tar content from 100 g/Nm$^3_{wet}$ to 83 g/Nm$^3_{wet}$. Benzene

Paper Received: 19 June 2021; Revised: 8 August 2021; Accepted: 5 September 2021
Please cite this article as: Harb R., Rivera-Tinoco R., Zeghondy B., Bouallou C., 2021, Modelling of Physical Method for Tar Elimination from Producer Gas at Low Temperature, Chemical Engineering Transactions, 88, 913-918 DOI:10.3303/CET2188152

and toluene remain in the producer gas after the scrubbers as seen in the gas composition in Table 1. Benzene and water will form a frost layer below 5.5 and 0°C, respectively, while toluene will condense as a liquid film.

Table 1: The composition of the producer gas after the water scrubbers.

Components	H_2	CO	CO_2	CH_4	C_2H_4	N_2	H_2O	C_6H_6	C_7H_8
Mole percentage (%)	38.57	23.09	18.99	8.33	2.20	5.15	0.90	2.44	0.33

The second unit targets the deposition of tars and water over cold surfaces. Many studies have handled the mechanism of frost formation and of condensation but separately. Most of these studies cover the deposition of water vapour present in the moist air for domestic or industrial applications, while none of them covers organic compounds, such as tar components. Simultaneous heat and mass transfer takes place during frost deposition and condensation. The formation of a frost layer limits the heat transfer due to its high thermal resistivity.
In this study, the simultaneous frosting and condensation phenomenon is considered to take place over a cold plate having a constant wall temperature. The multi-phase deposition process is explained in the first part. Then the equations governing the heat and mass transfer in the different sub-domains are presented. Finally, a parametric study is completed in order to analyse the impact of the gas flow rate and the wall temperature on the frosting parameters including the gas temperature, the frost thickness and the frost density.

2. Mathematical model of tar deposition

The producer gas is cooled by flowing over a cold plate whose temperature is lower than the dew point of the condensable components. Frost and liquid film will appear if the wall temperature is lower than the freezing point and the condensation point, respectively. Since studies tackling this simultaneous multi-component deposition-condensation do not exist, each phase is treated hypothetically separately. Therefore, two separate frost layers are considered, the first one for benzene and the second one for ice, in addition to a liquid toluene film that fills a certain volume from the pores. In this study, the producer gas flows through a duct where the upper plate is insulated to avoid the heat transfer between the gas and the environment. The process of frosting and condensation happens only on the lower plate of the duct, which is maintained at a constant low temperature. Figure 1 describes the physical model of heat and mass transfer between the gas and the condensable components. The process is divided into 6 subdomains: the gas, the interface between the ice frost layer and the gas, the ice frost layer, the interface between the ice and the benzene frost layers, the benzene frost layer and the toluene liquid volume.

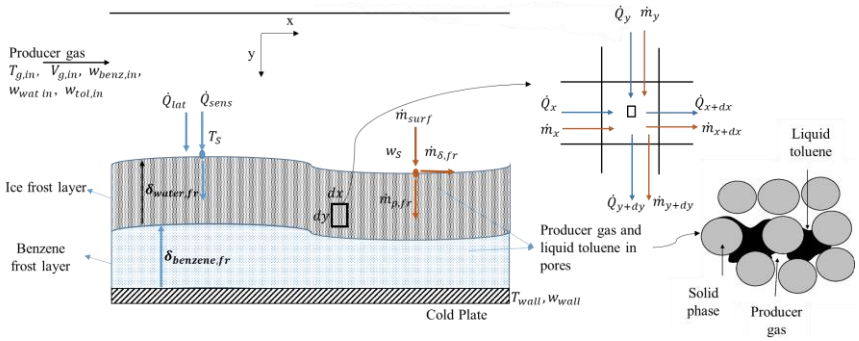

Figure 1: Frosting and condensation process diagram

Hayashi et al. (1977) work was among the first ones to study the frost growth process and divided it into three different periods; the “crystal growth period”, followed by the “frost layer growth period”, and finally the “frost layer full growth period”. The crystal growth period corresponds to the first moments of frost formation in the form of frost column. It is relatively short in time with respect to the whole frost formation process. To consider its impact on the frost growth, appropriate initial conditions, for the frost thickness ($\delta_{fr,int} = 2 \times 10^{-5}\ m$) and frost density ($\rho_{fr,int} = 25\ kg/m^3$), are considered (Lenic et al., 2009). The frost layer growth period is the most studied period during which the frost growth takes place in the form of a porous structure formed of a porous solid phase containing gaps filled by the producer gas. During this phase, the mass transferred from the gas phase to the cold surface is divided into two parts. The first one deposits on the surface of the frost and tends to increase the frost thickness, while the second one diffuses through the frost layer and contributes in increasing

the frost density (Wang et al., 2012). This continues until the surface temperature of the frost layer reaches the melting point of the condensable components, indicating the beginning of the frost layer full growth period. The developed mathematical model is formulated using 1D Cartesian coordinate system for the gas side and 2D Cartesian coordinate system for the condensate, it is discretized according to the finite volume method and implemented using Dymola.

2.1 Gas stream

Starting with the producer gas subdomain, the sensible heat transferred from the producer gas to the frost surface is calculated according to Eq(1).

$$\dot{Q}_{sensible} = h_{c,gas}.S.\left(T_{gas} - T_{frost,s}\right) \quad (1)$$

The total mass flow rates of benzene, water vapour and toluene, transferred from the producer gas to the frost surface, are calculated according to the heat and mass transfer analogy as in Eq(2) where $j \in \{\text{benzene, toluene, water vapour}\}$. Those mass flow rates will undergo a phase change. Benzene and water vapour are subject to frosting while toluene is subject to condensation.

$$\dot{m}_{s,j} = k_{m,j}.S.\rho_{gas}.\left(w_{gas,j} - w_{s,j}\right) \quad (2)$$

Note that the frost surface is considered at thermodynamic equilibrium. Thus the mass fraction at the frost surface can be linked to the saturation curves developed, in previous work (Harb et al., 2020 b), for each component at the surface temperate as follows: $w_{s,j} = f(T_{frost,s})$.

2.2 Frost surface

As mentioned previously, the total mass flow rate transfer from the gas to the frost surface ($\dot{m}_s$) is splitted into two terms. The first term ($\dot{m}_\delta$) corresponds to the mass flow rate that increases the frost thickness by deposition on the surface while the second term ($\dot{m}_\rho$) is the mass flow rate that increases the frost density by diffusion inside the frost. Eq(3) applies to the benzene and the ice frost layers.

$$\dot{m}_s = \dot{m}_\delta + \dot{m}_\rho \quad (3)$$

The mass flow rate that increases the frost density by diffusion inside the frost can be calculated function of the water vapour mass fraction variation along the y-axis at the surface and the effective diffusion coefficient of the water vapour in the gas of the frost pores as in Eq(4). Note that the effective diffusion coefficient is equal to the diffusion coefficient multiplied by the diffusion resistance factor (Le Gall et al., 1997).

$$\dot{m}_{\rho,water} = -D_{eff,water}.S.\rho_{gas}.(\partial w_{water}/\partial y)_s \quad (4)$$

Once the diffusing mass flow rate is calculated, the increasing thickness mass flow rate can be deduced from Eq(3). Therefore, the variation of the frost layer thickness can be calculated as follows:

$$\dot{m}_\delta = \rho_{frost}.S.(d\delta/dt) \quad (5)$$

The heat transfer at the frost surface can be expressed by Eq(6). The conductive heat transfer flow rate at the surface is calculated function of the temperature variation in the frost when y tends to $\delta_{fr,water}$ and the effective thermal conductivity of the frost (k_{eff}) as in Eq(7). Note that k_{eff} is calculated based on the correlation presented by Le Gall et al. (1997) based on the thermal conductivities of the solid and gas phase and the frost porosity.

$$\dot{Q}_{conductivity,water,s} = \dot{Q}_{sensible} + \dot{m}_{\delta,water}L_{sv,water} + \dot{m}_{s,toluene}L_{vap,toluene} \quad (6)$$

$$\dot{Q}_{conductivity,water,s} = -k_{eff,water}.S.(\partial T/\partial y)_s \quad (7)$$

2.3 Interface between the benzene and ice frost layers

The same equations for the mass fluxes apply to the benzene-ice interface. The difference between them is that the mass flux leading to the benzene frost densification is function of the benzene mass fraction variation at the interface. The total mass flow rate of benzene transferred from the gas to the benzene frost surface is calculated according to Eq(2). The benzene mass flow rate that increases the frost density by diffusion inside the frost can be calculated in Eq(8).

$$\dot{m}_{\rho,benzene} = -D_{eff,benzene}.S.\rho_{gas}.(\partial w_{benzene}/\partial y)_{interface} \quad (8)$$

Once the diffusing mass flow rate is calculated, the increasing thickness mass flow rate can be deduced from Eq(3). Then the variation of the benzene frost layer thickness ($d\delta/dt$) can be calculated from Eq(5).

The heat balance, at the interface between the two frost layers of benzene and ice, can be expressed by:

$$\left(-k_{eff,water}.S.(\partial T/\partial y)_{interface}\right) = \left(-k_{eff,benzene}.S.(\partial T/\partial y)_{interface}\right) + \dot{m}_{\delta,benzene}L_{sv,benzene} \quad (9)$$

2.4 Frost layer

The mass balance of benzene or water vapour inside the frost layers can be predicted according to Fick's law and it is expressed by:

$$\frac{\partial}{\partial x}\left(-D_{eff}.S.\rho_{gas}.\frac{\partial w}{\partial x}\right) + \frac{\partial}{\partial y}\left(-D_{eff}.S.\rho_{gas}.\frac{\partial w}{\partial y}\right) = -\alpha.S \quad (10)$$

Note that saturation condition is also considered inside the frost layer. Thus the same analogy discussed in the previous section applies also to the mass fraction gradient inside the frost layer.
The densification of the frost layers can be then calculated:

$$d\rho_{frost}/dt = \alpha \quad (11)$$

The energy balance inside the frost layer can then be applied according to Eq(12). The latter links between the heat transfer based on Fourier's law and the latent heat related to the mass densification.

$$\frac{\partial}{\partial x}\left(-k_{eff}.S.\frac{\partial T}{\partial x}\right) + \frac{\partial}{\partial y}\left(-k_{eff}.S.\frac{\partial T}{\partial y}\right) = \alpha.S.L_{sv} \quad (12)$$

2.5 Liquid toluene film

The volume fraction of the pores that will be filled by the liquid toluene is equal to the ratio of the accumulated volume of the condensed toluene to the volume of the frost pores as expressed in Eq(14).

$$v_{toluene} = \left(\dot{m}_{toluene,s}/\rho_{toluene}\right).t/\left(\left(\delta_{benzene,fr} + \delta_{water,fr}\right).S.\varepsilon\right) \quad (14)$$

3. Results and discussion

Models handling a simultaneous multi-component frosting and condensation do not exist. Thus the heat and mass transfer equations were first validated by comparing the results with different previous available studies for the case of water vapour frosting in humid air (Lee et al., 2003) as seen in Figure 2.

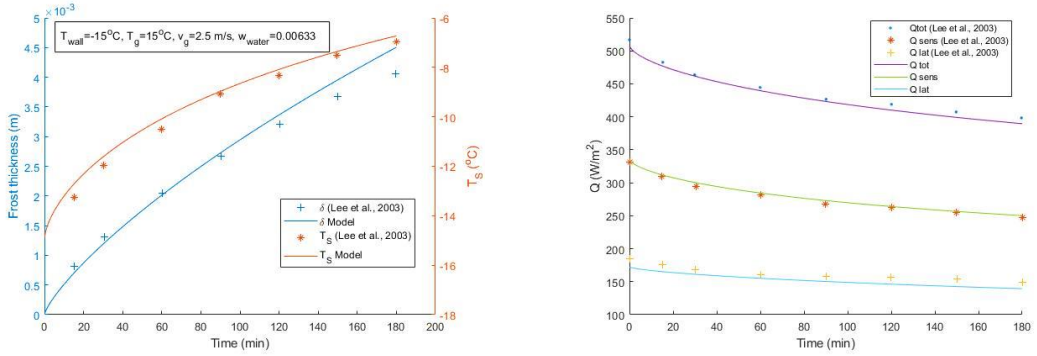

Figure 2: Validation of the frost growth model based on a comparison with Lee et al., (2003) for the variation of the frost layer thickness, frost surface temperature and heat fluxes over time

After validating the model, a parametric study is carried out. Table 2 summarises the different initial operating conditions considered for the parametric study. The initial mass fraction of the different condensable components is fixed for all the cases. Case 1 considers a low gas velocity (laminar flow), case 2 is similar to case 1 with higher velocity (turbulent flow). Case 3 has a low velocity with a higher wall temperature.

Figure 3 illustrates the variation of the gas temperature function of the plate length and the time, for the different inlet conditions shown in Table 2. It can be observed that, in all the cases, the gas temperature is decreasing along the plate length while it is increasing as the operating time increases. The lowest gas temperature at the end of the plate is reached in case 1, while the highest one is encountered in case 3. In addition, the gas

temperature variations in case 1 and case 2 are very close. However, it can be seen that in case 1, the rate of increase of the gas temperature, function of time, at the end of the plate, is lower than that of case 2.

Table 2: Different inlet conditions considered for the parametric study

Case	T_{wall} (℃)	T_g (℃)	$w_{benzene}$	$w_{toluene}$	w_{water}	v_g (m/s)	Plate dimensions $w \times h \times L$ (m^3)
1	-20	5	0.089	0.0142	0.0075	0.6	$0.05 \times 0.05 \times 5$
2	-20	5	0.089	0.0142	0.0075	1	$0.05 \times 0.05 \times 5$
3	-10	5	0.089	0.0142	0.0075	0.6	$0.05 \times 0.05 \times 5$

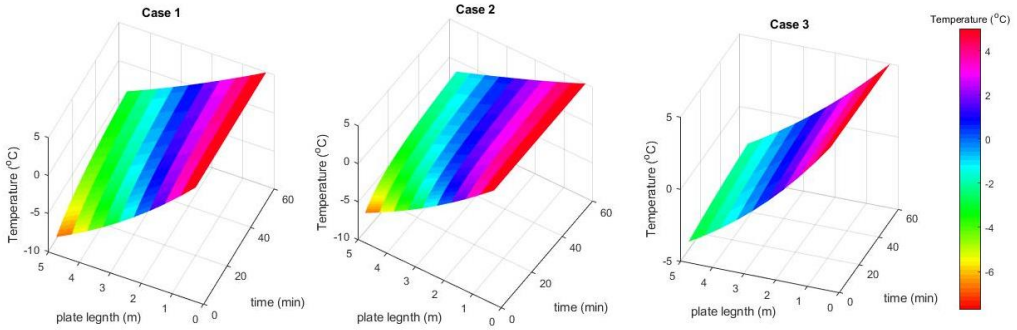

Figure 3: Variation of the gas temperature function of the plate length and the time for different initial conditions

Figure 4 presents the variation of the benzene and ice frost thicknesses function of the plate length and the time, for the different inlet conditions shown in Table 2. It can be observed that benzene frost thickness is increasing along the plate length and with respect to the operating time, in all the cases except case 3. In the latter, the difference between the gas temperature and the wall temperature is not high enough to promote the mass transfer and consequently thicken the initial benzene frost layer. The deposited weight of benzene is low and therefore, it is only leading to density increase. The ice frost thickness is increasing with respect to the operating time while it is decreasing along the plate length, in all the cases. Note that, due to the accumulation of the total frost thickness function of time, the resistivity of the frost thickness is increasing leading to an increase in the gas temperature with time. Even though the initial content of benzene is higher than that of water, the ice frost layer is thicker than the benzene frost layer. This is related to the saturation vapour pressure which is higher for benzene.

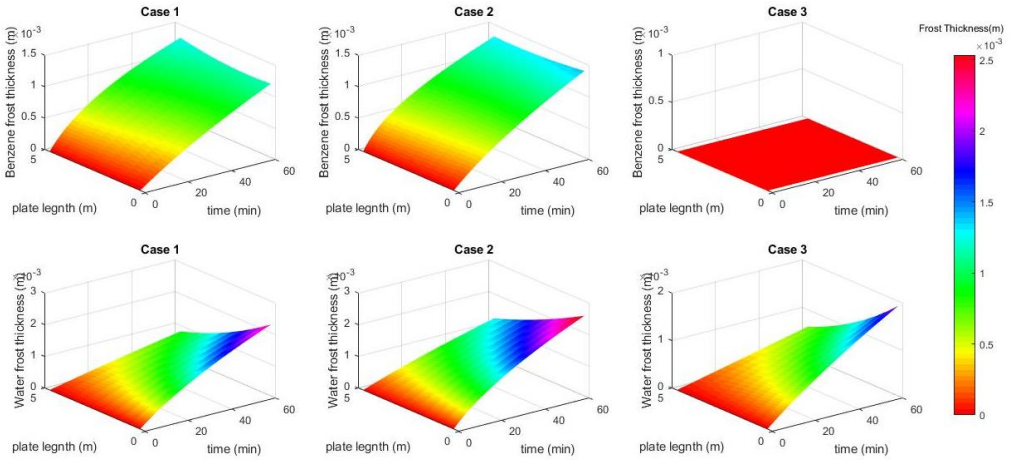

Figure 4: Variation of the benzene and ice frost thicknesses function of the plate length and the time for different initial conditions

As for the frost density, in both sub-domains, the density is higher at the front end of the plate where the producer gas with high tar content enters. The density decreases towards the rear end of the cooling surface. In general,

the density is higher near the cold surface and it decreases towards the frost surface. As the frost layer grows, the distance between the cold surface and the frost surface increases, leading to an increase in the thermal resistance. Therefore, the frost surface and the gas temperatures increase. This general behavior of densification is encountered in all the cases but it is less important in case 3 where the temperature difference is not high enough to sharply increase the density. Based on the model results, it can be seen that benzene frost is denser than the ice frost due to its higher initial mass fraction. After 60 minutes, the benzene frost density is equal to 90 and 120 kg/m^3 at the beginning of the plate and it decreases to 40 and 50 kg/m^3 at the end of the plate in case 1 and case 2, respectively. As for the ice frost density, it is equal to 40 and 45 kg/m^3 at the beginning of the plate and it decreases to 26 and 30 kg/m^3 at the end of the plate in case 1 and case 2, respectively. In case 3, the benzene and ice frost densities remain constant around 35 and 30 kg/m^3, respectively.

4. Conclusions

The mathematical model of simultaneous frost growth and condensation is developed on Dymola, while the properties of the mixtures are extracted from Aspen Properties. The results of the sensitivity study showed that a temperature difference of 15°C between the wall and the gas inlet is not sufficient to lead to benzene frosting nor to reduce its content in the producer gas. Comparing case 1 to case 2, the latter has a higher velocity therefore higher turbulence. The gas temperature, after 60 minutes of operation, is reduced to -3.5°C in case 1, while in case 2 to -1.5°C. Consequently, the benzene content is reduced to 0.075 in case 1 and to 0.0784 in case 2. The content of toluene was not importantly affected by condensation. Thus a lower temperature is required. A future improvement to reduce the remaining content could be placing several plates in series having decreasing wall temperatures until reaching the required target.

Nomenclature

D_{eff} – effective diffusion coefficient, m^2/s
h_c – convective heat transfer coefficient, W/(m^2·K)
k_{eff} – effective thermal conductivity, W/(m·K)
k_m – mass transfer coefficient, m/s
L_{sv} – latent heat of sublimation, J/kg
L_{vap} – latent heat of evaporation, J/kg
$\dot{m}$ – mass flow rate, kg/s
$\dot{Q}$ – heat transfer rate, W
S – gas side heat transfer area, m^2
s – surface
t – time, s
T – Temperature, °C
v_g – gas velocity, m/s
$v_{toluene}$ – relative volume, -
w – mass fraction, -
α – absorption rate, kg/(m^3·s)
δ – frost thickness, m
ρ – density, kg/m^3
ε – porosity, -

References

Anis S., Zainal Z.A., 2011, Tar reduction in biomass producer gas via mechanical, catalytic and thermal methods: A review. Renewable and Sustainable Energy Reviews, 15, 2355–2377.

Harb R., Rivera-Tinoco R., Nemer M., Zeghondy B., Bouallou C., 2020a, Process Simulation of Tar Removal from Gasification Producer Gas. Chemical Engineering Transactions, 81, 6.

Harb R., Rivera-Tinoco R., Nemer M., Zeghondy B., Bouallou C. 2020b, Towards synthetic fuels production from biomass gasification: Tar content at low temperatures. Biomass and Bioenergy, 137, 105540.

Hayashi Y., Aoki A., Adachi S., Hori K., 1977, Study of Frost Properties Correlating With Frost Formation Types. Journal of Heat Transfer, 99, 239–245.

Lee K-S., Jhee S., Yang D-K., 2003, Prediction of the frost formation on a cold flat surface. Int J Heat Mass Transfer, 46 (20), 3789–96.

Le Gall R., Grillot J.M., and Jallut C., 1997, Modelling of Frost Growth and Densification. International Journal of Heat and Mass Transfer, 40 (13), 3177–87.

Lenic K., Trp A., Frankovic B., 2009, Transient two-dimensional model of frost formation on a fin-and-tube heat exchanger. International Journal of Heat and Mass Transfer, 52, 22–32.

Phuphuakrat T., Namioka T., Yoshikawa K., 2011, Absorptive removal of biomass tar using water and oily materials. Bioresource Technology, 102, 543–549.

Thunman H., Seemann M., Vilches T. B., Maric J., Pallares D., Ström H., Berndes G., Knutsson P., Larsson A., Breitholtz C., Santos O., 2018, Advanced biofuel production via gasification – lessons learned from 200 man-years of research activity with Chalmers' research gasifier and the GoBiGas demonstration plant. Energy Science & Engineering, 6, 6–34.

Wang W., Guo Q. C., Lu W. P., Feng Y. C., Na W., 2012, A generalized simple model for predicting frost growth on cold flat plate. International Journal of Refrigeration, 35, 475–486.